Physics of the Earth and Planetary Interiors 171 (2008) 296–312

Contents lists available at ScienceDirect

Physics of the Earth and Planetary Interiors

journal homepage: www.elsevier.com/locate/pepi

Subduction initiation by thermal–chemical plumes: Numerical studies

Kosuke Ueda [a,b,*], Taras Gerya [b,1], Stephan V. Sobolev [c,d,2]

[a] Department of Earth Science, University of Bergen, Allégaten 41, 5007 Bergen, Norway
[b] Department of Earth Sciences, ETH-Zurich, ETH-Hoenggerberg, HPP, 8093 Zurich, Switzerland
[c] GeoForschungsZentrum Potsdam (GFZ), Telegraphenberg, 14473 Potsdam, Germany
[d] Schmidt Institute of Physics of the Earth, B. Gruzinskaya 10, Moscow, Russia

ARTICLE INFO

Article history:
Received 30 October 2007
Received in revised form 20 May 2008
Accepted 30 June 2008

Keywords:
Subduction initiation
Thermal–chemical plume
Numerical modelling
Plate strength

ABSTRACT

Prior suggestions for the initiation of subduction have included sediment loading, compression, and plate reconfiguration as potential triggers. Here, we investigate the possibility of subduction initiation by the interaction of the lithosphere with a buoyant mantle plume. Numerical testing of this hypothesis has been conducted in 2D with the I2VIS thermo-mechanical code accounting for phase transitions and a viscoplastic model of a thin oceanic lithosphere hit by a partially molten thermal–chemical or purely thermal plume. We demonstrate that a mantle plume can break the lithosphere and initiate self-sustaining subduction, provided the plume causes a critical local weakening of the lithospheric material above it. The intensity of the required weakening depends on the plume volume, plume buoyancy, and the thickness of the lithosphere and is the highest for the least buoyant purely thermal plumes. Another necessary condition is the presence of high-pressure fluids at the slab upper interface, reducing the effective friction coefficient there to very low values. Based on our results, we suggest that sheet-like instabilities of the Archean mantle convection could have initiated subduction on Earth where ocean was already present in less stable tectonic settings, provided that mantle plumes (sheets) at that time were rich in water and melt, which could drastically reduce the effective friction coefficient in the lithosphere above the plume. Our numerical models are also in good agreement with suggested concepts for corona formation on Venus.
© 2008 Elsevier B.V. All rights reserved.

1. Introduction

Earth's current tectonics are characterized by subduction as a major process for accommodating plate convergence within a probably unique framework of planetary convection. Subduction becomes self-sustaining after a certain initiation phase, but it seems to be very difficult to initiate this process. Although studied to some extent (McKenzie, 1977; Turcotte et al., 1977; Cloetingh et al., 1989; Ogawa, 1990; Mueller and Phillips, 1991; Sandwell and Schubert, 1992; Kemp and Stevenson, 1996; Toth and Gurnis, 1998; Regenauer-Lieb et al., 2001; Solomatov, 2004), the physical understanding (e.g., Fowler, 1993) of the exact conditions and requirements of such initiation is still missing. Starting from an intact plate where the plate boundary of the new subduction zone is not predefined (e.g., Gurnis and Hager, 1988), there are two major prerequisites: first, the cohesion of the lithosphere has to be overcome by some means to localize a plate boundary and to focus stresses; second, the vertical movement of slabs and the related bending has to be activated or facilitated. Several mechanisms have been proposed for each of these issues, whereas the localization of a plate boundary deformation seems to be the largest problem (McKenzie, 1977; Mueller and Phillips, 1991).

Failure of the plate needs to be facilitated, either by global weakening of the lithosphere (e.g., Solomatov, 2004), by an inherited lithospheric weak zone (fault system) (McKenzie, 1977; Mueller and Phillips, 1991; Toth and Gurnis, 1998; Hall et al., 2003), by conversion of different plate boundaries (Mueller and Phillips, 1991; Gurnis et al., 2004), by deep thermal cracking and hydration (Korenaga, 2007), or through (thermal-)mechanical feedback mechanisms with dynamic rheologies (Regenauer Lieb and Yuen David, 2000; Branlund et al., 2001), including weakening effects of water (Regenauer-Lieb et al., 2001). Far-field compression (Han and Gurnis, 1999; Hall et al., 2003), and especially an increase in compression, are also claimed to be able to trigger the high stresses that are believed to be required for the initiation of subduction (McKenzie, 1977; Mueller and Phillips, 1991). Such compression may occur, for example, as a result of the formation of new spreading ridges (Cloetingh et al., 1989), or when buoyant lithosphere congests at trenches (Mueller and Phillips, 1991), building up

* Corresponding author. Tel.: +47 55 58 3516; fax: +47 55 58 3600.
E-mail addresses: kosuke.ueda@geo.uib.no (K. Ueda), taras.gerya@erdw.ethz.ch (T. Gerya), stephan@gfz-potsdam.de (S.V. Sobolev).
[1] Tel.: +41 44 6336623; fax: +41 44 6331065.
[2] Tel.: +49 331 288 1248; fax: +49 331 288 1266.

0031-9201/$ – see front matter © 2008 Elsevier B.V. All rights reserved.
doi:10.1016/j.pepi.2008.06.032

stresses to locate subduction elsewhere (Stern, 2004). However, such a reconfiguration model describes the initiation of subduction at one place when another place becomes unfavourable, but leaves the question of the origin of subduction unanswered. In addition, failure can be driven or facilitated by sedimentary loading stresses (Cloetingh et al., 1989; Mueller and Phillips, 1991; Regenauer-Lieb et al., 2001; Branlund et al., 2001), by spontaneous thrusting of the buoyant continental crust over the oceanic crust (Mart et al., 2005), by small-scale convection in the sub-lithospheric mantle (Solomatov, 2004), or by external tension exerted on a passive margin (Kemp and Stevenson, 1996). Many of these possibilities can be combined.

On the other hand, the onset of downward movement (foundering) seems to be much easier to trigger, since cooling naturally decreases the buoyancy of lithosphere, soon leading to a metastable, negatively buoyant lithosphere. Additional down-warp can be produced by flexural response to compression (Hall et al., 2003), by bottom pull of cold convective lithospheric instabilities (Ogawa, 1990), or by top loading at passive margins (Cloetingh et al., 1989; Mueller and Phillips, 1991; Regenauer-Lieb et al., 2001; Branlund et al., 2001). Loading can also be magmatic (Kemp and Stevenson, 1996), if tension-induced passive rifting leads to mantle flow over a lithosphere edge.

Apart from the mechanisms above, subduction seems to be generally favoured by the presence of water in slabs and/or mantle (Lenardic and Kaula, 1994; Regenauer-Lieb et al., 2001; Solomatov, 2004; Gerya et al., 2008; Van der Lee et al., 2008). Some influences like external compression, strong tension, or strong sediment loads can likely facilitate both lithosphere failure and down-warp, and are thus promising for modelling using fully dynamic approaches and realistic lithospheric rheology.

In this study, we investigate the possibility of initiating the subduction of thin (young or simply hot), unforced oceanic lithosphere following the impingement of a buoyant thermal–chemical or purely thermal mantle plume. The potential of such initiation is related to (i) high stresses and large deformation, which can be produced in the lithosphere due to its interaction with strongly positively buoyant thermal–chemical mantle (e.g., Burov and Guillou-Frottier, 2005; d'Acremont et al., 2003;), and to (ii) possible magmatic loading (cf. Kemp and Stevenson, 1996) if plumes are able to reach the surface.

Although no geologic record supporting subduction following plume impingement currently exists, this mechanism could also have been developed in earlier stages of planetary evolution. However, modes and conditions of, for instance, Archean tectonics are still relatively unconstrained (Griffin et al., 2003; Brown, 2006). Early Archean tectonics were probably dominated by impacts and catastrophic revolutions, while towards the later Archean, more modern-like tectonics subsequently took over (Brown, 2006, 2007). The transition is relatively unconstrained; apparently, coexisting modern-type processes like steeper subduction with the duality of metamorphic conditions in orogenic belts have gained increasing importance (e.g., Smithies et al., 2005; Sol et al., 2002; Brown, 2006, 2007). It is thus not the primary goal of this study to reproduce plume–lithosphere interactions in a specific setting, but it is rather to validate the possibility and requirements to initiate the subduction of oceanic lithosphere by mantle plumes when both have starting properties close to that of the present-day Earth.

The present numerical study addresses the response of thin oceanic lithosphere to a thermal–chemical plume in a two-dimensional representation. It seems debatable whether the impingement of a plume (usually cylindrical) leading to the initiation of a subduction zone (a strongly elongated effect) is properly represented in a 2D-model. However, patterns of primary sheet-like perturbations or elongated, lateral interference patterns of composite plumes are reported from numerical modelling (Ismail-Zadeh et al., 2006; Kaus and Podlachikov, 2001) and may have a present-day equivalent in the shape of the African super plume as inferred from seismic tomography (Ni et al., 2002, 2005). In addition, some tectonic plates might have temporarily evolved to reasonably small sizes (e.g., Juan de Fuca plate, Gorda plate, Explorer plate), even down to a scale such that the length of a developing trench would not be a multiple of the diameter of the plume. We therefore believe that, for a principal starting point, it is sufficiently justifiable to assume first-order homogeneity of our geometry in the third dimension. To check the dependence of our results on various physical parameters, we performed qualitative comparisons with additional series of model runs.

2. Numerical model

2.1. Initial model setup

The model dimensions are 2000 km × 200 km, distributed over 521 × 101 grid nodes. The grid resolution is non-uniform: 2 km × 2 km in the central 800 km × 200 km part of the model and 10 km × 2 km on the model sides where no significant deformation occurs. A large amount (ca. two million) of markers allows for high resolution of the lithological field. The initial geometry of the model (Fig. 1a) corresponds to the onset of interaction of a rising plume with the young oceanic lithosphere. To reproduce this lithosphere, we have chosen a common layered model from the uppermost mantle to the surface. The crustal part is represented by sediments (0.5 km), altered basalts (1.5 km), and gabbroic rocks (5 km) as in the typical present-day oceanic lithosphere. The lithospheric and asthenospheric mantle is modelled as anhydrous peridotite, extending as a half-space to the lower boundary of the model (Table 1). This setup is complemented by 3 km of water above. The impinging plume is produced by placing a circular volume of partially molten material (of varied composition, water content and temperature, see Table 2) in depth (mid-point at $z = 125$ km) into the mantle, which deforms into the desired mushroom-head shape during its rise through the mantle. By default, we use a plume consisting of hydrated mantle material (Table 1) with a temperature of 1700 K. The coordinate system has its origin in the left-upper corner, with the depth z increasing downwards, so that the surface of the crust is at $z = 15$ km. For the convenience of viewing, we have limited the field of view to the central 500 km and shown local width with $X = 0$ at the left end of the close-up (corresponding to a global position of $x = 750$ km).

The initial temperature field in the lithospheric plate is defined by an oceanic geotherm (Turcotte and Schubert, 2002) with a prescribed lithospheric age, which was varied from 1 to 15 Ma (Table 2) in different numerical experiments. The initial temperature of the asthenospheric mantle at $z = 100$ km depth is 1377 °C and the vertical temperature gradient below $z = 100$ km depth is 0.5 °C/km as in the typical present-day oceanic asthenosphere. The base of the lithosphere is not defined by a rheological boundary, but results from temperature-dependent densities and effective viscosities. An approximate thickness of the lithosphere for different experiments is given in Table 2 corresponding to the depth of the 1200 K isotherm below the surface.

2.2. Boundary conditions

We implemented free slip conditions at all boundaries except at the lower boundary, which is permeable in both the downward and upwards directions. Infinite-like *external free slip conditions* (Burg

and Gerya, 2005) along the bottom imply that the free slip condition is satisfied at an *external boundary* located at a certain depth below the actual lower boundary of the model (at the depth of 1000 km below the lower boundary for our study). Similar to the usual free slip condition, external free slip allows global conservation of mass in the computational domain and is implemented by using the following limitation for velocity components at the lower boundary:

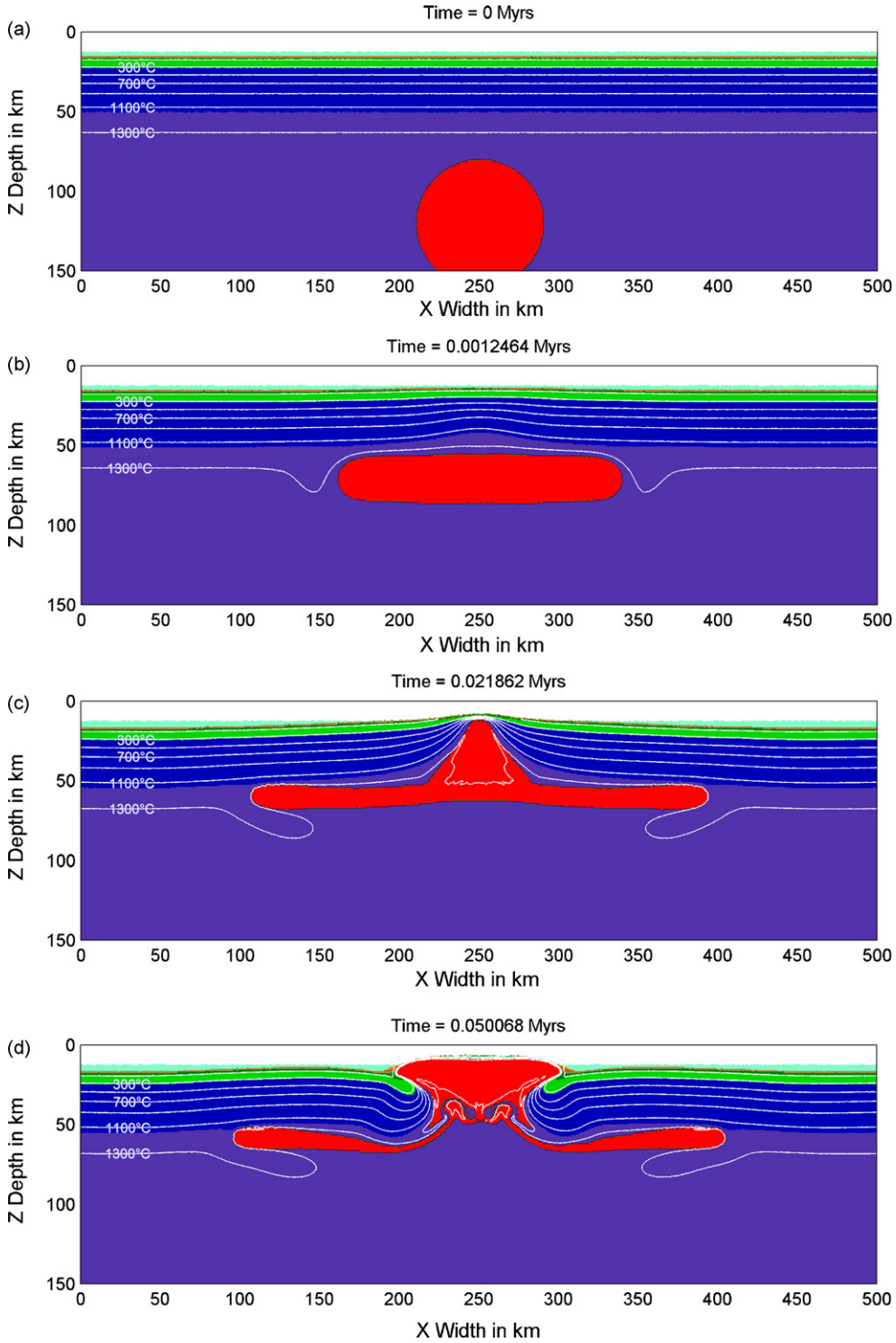

Fig. 1. Reference case of plume–lithosphere interaction (model 1). (a) Initial setup, plume modelled as circular volume of hydrated partially molten rocks in the mantle. (b) Spreading of the plume at the base of the lithosphere. (c) Development of a central plume wedge that rises through the lithosphere. (d) Once the partially molten wedge passed the lithosphere, it starts to spread. At the same time, remnants of the earlier flattening plume become divided into two separate sheets at the lithosphere base (underplating). (e) Subduction starts and (f) continues to be self-sustaining and retreating. (g) At a certain degree of steepening, the shallow slab breaks off over the plume remnants. (h) After break-off of both slabs, ~400 km of new ocean floor is created. The lithospheric and asthenospheric mantles have the same physical properties (Table 1), different colours are used only for visualizing slab deformation and structural development. (For interpretation of the references to colour in this figure legend, the reader is referred to the web version of the article.)

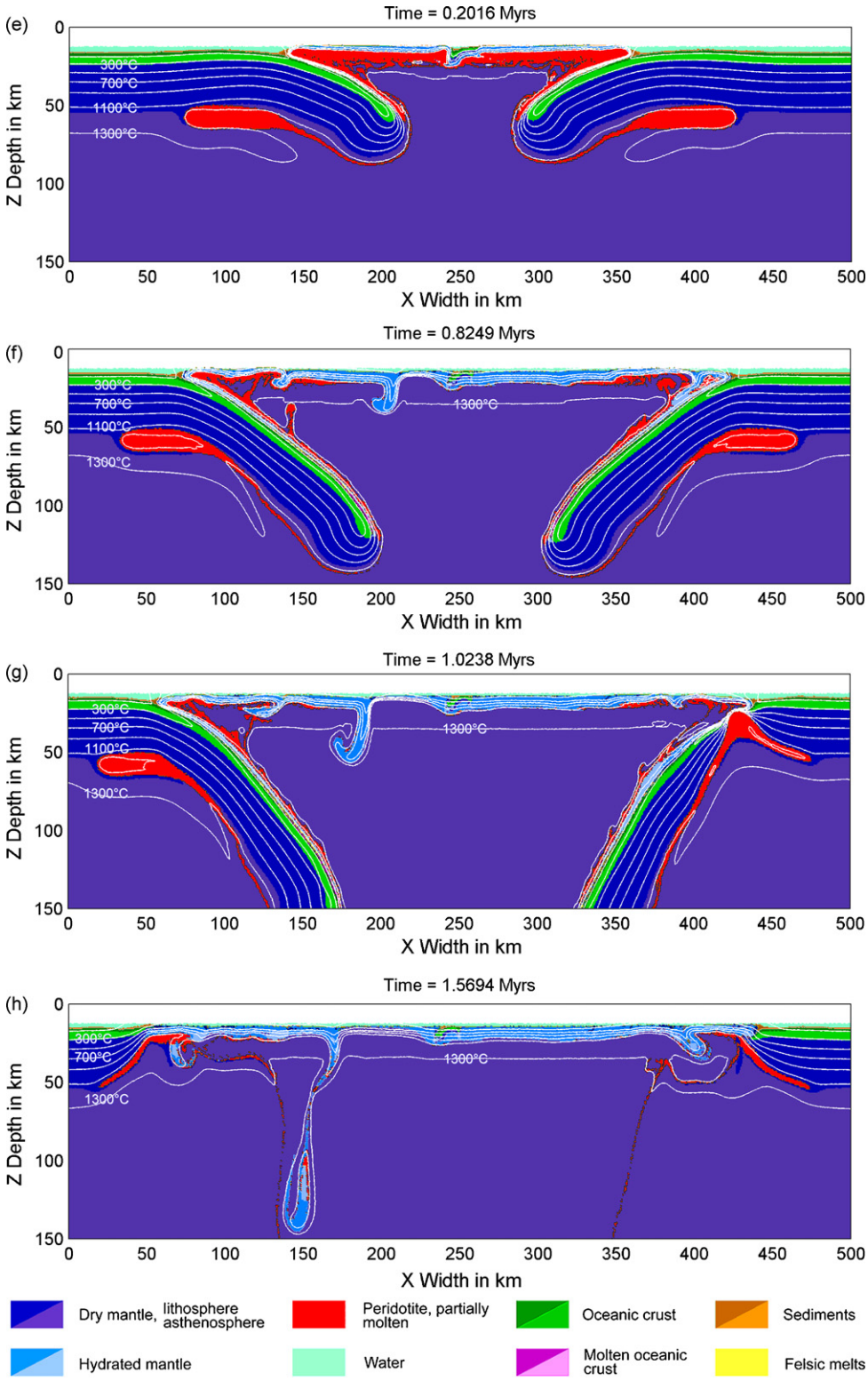

Fig. 1. (*Continued*).

$$\frac{\partial v_x}{\partial z} = 0,$$

$$\frac{\partial v_z}{\partial z} = -\frac{v_z}{\Delta z_{\text{external}}}$$

where $\Delta z_{\text{external}}$ is the vertical distance from the bottom of the model to the external boundary where free slip ($\partial v_x/\partial z = 0$, $v_z = 0$) is satisfied (i.e., $\Delta z_{\text{external}} = 1000$ km for the present study). In order to minimize mechanical interaction of cold slabs with the permeable lower boundary, the maximal viscosity at the 20 km deep region along this boundary was limited to 10^{19} Pa s. An *external constant*

Table 1
Material properties used in numerical experiments

Material[a]	Maximal water content in hydrous minerals (wt.%)	Thermal conductivity (W/(m K))	H_r (μW/m^3)	Flow law	E (kJ/mol)	n	A_D (MPa^{-n} s^{-1})	c (MPa)	sin(φ)	P–T conditions of wet solidus
Sediment, felcis rock	7.6	$0.64+807/(T+77)$	1–1.75	Wet quartzite	154	2.3	$10^{-3.5}$	3–10	0	$889+(17900/(P+54))+(20200/(P+54)^2)$ at $P<1200$ MPa, $831+0.06P$ at $P>1200$ MPa
Upper oceanic crust (altered basalt)	2.8	$1.18+474/(T+77)$	0.25	–//–	–//–	–//–	–//–	3–10	0	$973-(70400/(P+354))+(77800000/(P+354)^2)$ at $P<1600$ MPa, $935+0.0035P+0.0000062P^2$ at $P>1600$ MPa
Lower oceanic crust (gabbro)	1.5	–//–	0.022	Plagioclase An_{75}	238	3.2	$10^{-3.5}$	3	0.05–06	–//–
Hydrated mantle	2.0	$0.73+1293/(T+77)$	0.022	Wet olivine	470	4	$10^{3.3}$	3	0	$1240+(49800/(P+323))$ at $P<2400$ MPa, $1266-0.0118P+0.0000035P^2$ at $P>2400$ MPa
Dry mantle (lithosphere, asthenosphere)	0	–//–	0.022	Dry olivine	532	3.5	$10^{4.4}$	3	0.05–0.6	–
References	Gerya et al. (2006)	Clauser and Huenges (1995)	Turcotte and Schubert (2002)	Ranalli (1995)						Schmidt and Poli (1998); Poli and Schmidt (2002)

[a] Model rock compositions, wt.% (Gerya et al., 2006): sediment – SiO_2 = 61.10, Al_2O_3 = 12.43, FeO = 5.43, MgO = 2.59, CaO = 6.21, Na_2O = 2.54, K_2O = 2.13; basalt – SiO_2 = 47.62, Al_2O_3 = 14.48, FeO = 10.41, MgO = 6.92, CaO = 13.39, Na_2O = 2.15, K_2O = 0.58; gabbro – SiO_2 = 53.49, Al_2O_3 = 14.07, FeO = 6.86, MgO = 12.07, CaO = 10.73, Na_2O = 1.22, K_2O = 0.09; mantle – SiO_2 = 45.55, Al_2O_3 = 4.03, FeO = 7.47, MgO = 37.42, CaO = 3.18, Na_2O = 0.33, K_2O = 0.03.

temperature condition which simulates an infinite half-space along the bottom of the model (*infinite-like condition*) is implemented by using the following limitation:

$$\frac{\partial T}{\partial z} = \frac{T_{\text{external}} - T}{\Delta z_{\text{external}}},$$

where T_{external} = 1723 °C is the temperature at the external boundary. The temperature gradient along the bottom of the model is thus not fixed and varies with time in response to the variations in the mantle temperature above this boundary (e.g., due to subducting slab propagation).

The top surface of the oceanic crust is calculated dynamically as an internal free surface by initially using a 15 km-thick top layer with a low viscosity (10^{19} Pa s) and density (1 kg/m^3 for the atmosphere, 1000 kg/m^3 for seawater prescribed in the weak layer below z = 12 km water level). The interface between this weak layer and the top of the oceanic crust deforms spontaneously and is treated as an erosion/sedimentation surface that evolves according to the transport equation (in Eulerian coordinates) solved at each time-step (Gerya and Yuen, 2003b)

$$\frac{\partial z_{es}}{\partial t} = v_z - v_x \frac{\partial z_{es}}{\partial x} - v_s + v_e \quad (1)$$

where z_{es} is a vertical position of the surface as a function of the horizontal distance x; v_z and v_x are the vertical and horizontal components of the material velocity vector at the surface; v_s and v_e are the gross scale sedimentation and erosion rates, respectively, which correspond to the relation:

$$v_s = 0, \quad v_e = 0.3\,\text{mm/year} \qquad \text{when } z < 12\,\text{km},$$

$$v_s = 0.03\,\text{mm/year}, \quad v_e = 0 \qquad \text{when } z > 12\,\text{km}.$$

Erosion and sedimentation processes are implemented via a marker transmutation. The low viscosity of the weak top layer (10^{19} Pa s) creates a high viscosity contrast (>10^3) and causes minimal shear stresses (<10^4 Pa) along the erosion/sedimentation surface (Burg and Gerya, 2005). Test experiments have shown that choosing lower viscosities of the weak layer does not notably affect the gross scale model development.

2.3. Petrological model

Mineralogical phase transformations such as dehydration reactions, melting, and eclogitization of subducted crust can significantly affect the physical properties of rocks. In order to account for these effects, we used a coupled petrological–thermo-mechanical numerical modelling approach described in detail by Gerya et al. (2004, 2006). According to this approach, all *in situ* rock properties, including effective density, isobaric heat capacity, thermal expansion, adiabatic and latent heating as well as equilibrium water and melt content are calculated for Lagrangian rock markers at every time step based on taking the Gibbs free energy minimization (Connolly and Petrini, 2002) as a function of local pressure, temperature and rock composition (Table 1). Thermodynamic properties of fluids, melts, and minerals for this calculation are taken from an internally consistent thermodynamic database (Gerya et al., 2006). To calculate the physical properties for a large amount of rock markers, we used reference tables pre-computed for each lithology where phase relations were resolved in P–T space on a grid with a resolution of 5 K and 25 MPa. Examples of phase diagrams computed for different lithologies are discussed by Kerrick and Connolly (2002). The range of physical and chemical conditions considered here requires extrapolation of the silicate melt model (Ghiorso et al., 2002). Therefore, to ensure consistency with experimentally constrained melting boundaries (Table 1) employed in our earlier work

Table 2
Parameters of conducted numerical experiments

Model	Plume radius (km)	Age of lithosphere (Ma)	Approx. lithosphere thickness (km)	Temperature of plume (K)	Plume composition	Density contrast lithosphere–plume (kg/m^3)			Plastic strength lithosp. mantle ($\sin(\varphi)$ in Eq. (5))	Mobility melt/fluid	Result[a]
						Thermal (thermal expansion)	Chemical (water, melts, mineralogy)	Total			
1 (pr11)	40	10	41	1700	Hyd. mantle	94	275	369	0.1	y/y	O
2 (pr12)	38	10	41	1700	Hyd. mantle	94	275	369	0.1	y/y	C
3 (pr13)	36	10	41	1700	Hyd. mantle	94	275	369	0.1	y/y	X
4 (pr14)	50	5	41	1700	Hyd. mantle	94	275	369	0.1	y/y	O
5 (pr15)	40	5	29	1700	Hyd. mantle	94	275	369	0.1	y/y	O
6 (pr16)	30	5	29	1700	Hyd. mantle	94	275	369	0.1	y/y	X
7 (pr17)	20	5	29	1700	Hyd. mantle	94	275	369	0.1	y/y	X
8 (pr18)	15	5	29	1700	Hyd. mantle	94	275	369	0.1	y/y	X
9 (pr19)	32	5	29	1700	Hyd. mantle	94	275	369	0.1	y/y	O
10 (pr20)	70	10	41	1700	Hyd. mantle	94	275	369	0.1	y/y	O
11 (pr21)	32	10	41	1700	Hyd. mantle	94	275	369	0.1	y/y	X
12 (pr22)	40	7.5	35.5	1700	Hyd. mantle	94	275	369	0.1	y/y	O
13 (pr23)	36	7.5	35.5	1700	Hyd. mantle	94	275	369	0.1	y/y	O
14 (pr24)	32	7.5	35.5	1700	Hyd. mantle	94	275	369	0.1	y/y	X
15 (pr25)	30	7.5	35.5	1700	Hyd. mantle	94	275	369	0.1	y/y	X
16 (pr26)	26	7.5	35.5	1700	Hyd. mantle	94	275	369	0.1	y/y	X
17 (pr27)	50	15	50.5	1700	Hyd. mantle	94	275	369	0.1	y/y	O
18 (pr28)	45	15	50.5	1700	Hyd. mantle	94	275	369	0.1	y/y	O
19 (pr29)	40	15	50.5	1700	Hyd. mantle	94	275	369	0.1	y/y	X
20 (pr30)	35	15	50.5	1700	Hyd. mantle	94	275	369	0.1	y/y	X
21 (pr31)	31	5	29	1700	Hyd. mantle	94	275	369	0.1	y/y	O
22 (pr32)	34	7.5	35.5	1700	Hyd. mantle	94	275	369	0.1	y/y	X
23 (pr33)	42	15	50.5	1700	Hyd. mantle	94	275	369	0.1	y/y	X
24 (pr34)	37	10	41	1700	Hyd. mantle	94	275	369	0.1	y/y	X
25 (pr35)	30	2	18.5	1700	Hyd. mantle	94	275	369	0.1	y/y	<>
26 (pr36)	28	2	18.5	1700	Hyd. mantle	94	275	369	0.1	y/y	<>
27 (pr37)	26	2	18.5	1700	Hyd. mantle	94	275	369	0.1	y/y	X
28 (pr38)	27	2	18.5	1700	Hyd. mantle	94	275	369	0.1	y/y	C
29 (pr39)	43	15	50.5	1700	Hyd. mantle	94	275	369	0.1	y/y	O
30 (pr40)	37.5	10	41	1700	Hyd. mantle	94	275	369	0.1	y/y	X
31 (pr41)	41	12.5	46	1700	Hyd. mantle	94	275	369	0.1	y/y	C
32 (pr42)	42	12.5	46	1700	Hyd. mantle	94	275	369	0.1	y/y	O
33 (pr43)	40	12.5	46	1700	Hyd. mantle	94	275	369	0.1	y/y	X
34 (pc44)	36	10	41	1700	Mafic	94	165	259	0.1	y/y	X
35 (pc45)	38	10	41	1700	Mafic	94	165	259	0.1	y/y	X
36 (pc46)	40	10	41	1700	Mafic	94	165	259	0.1	y/y	X
37 (pc47)	36	10	41	1700	Felsic	94	800	894	0.1	y/y	O
38 (pc48)	38	10	41	1700	Felsic	94	800	894	0.1	y/y	O
39 (pc49)	40	10	41	1700	Felsic	94	800	894	0.1	y/y	O
40 (pt50)	38	10	41	1800	Hyd. mantle	104	275	379	0.1	y/y	C
41 (pt51)	35	10	41	1800	Hyd. mantle	104	275	379	0.1	y/y	X
42 (pt52)	32	10	41	1800	Hyd. mantle	104	275	379	0.1	y/y	X
43 (pt53)	36	10	41	1600	Hyd. mantle	84	275	359	0.1	y/y	X
44 (pt54)	38	10	41	1600	Hyd. mantle	84	275	359	0.1	y/y	O
45 (pt55)	40	10	41	1600	Hyd. mantle	84	275	359	0.1	y/y	O
46 (ps56)	38	10	41	1700	Hyd. mantle	94	275	369	0.05	y/y	X ctbd
47 (ps57)	37	10	41	1700	Hyd. mantle	94	275	369	0.05	y/y	X ctbd
48 (ps58)	36	10	41	1700	Hyd. mantle	94	275	369	0.05	y/y	X ctbd
49 (ps59)	38	10	41	1700	Hyd. mantle	94	275	369	0.15	y/y	X ctbd
50 (ps60)	39	10	41	1700	Hyd. mantle	94	275	369	0.15	y/y	X ctbd
51 (ps61)	40	10	41	1700	Hyd. mantle	94	275	369	0.15	y/y	X ctbd
52 (pw62)	40	10	41	1700	Hyd. mantle	94	275	369	0.1	n/y	O
53 (pw63)	36	7.5	35.5	1700	Hyd. mantle	94	275	369	0.1	n/y	O
54 (pw64)	38	10	41	1700	Hyd. mantle	94	275	369	0.1	n/y	O
55 (pw62b)	40	10	41	1700	Hyd. mantle	94	275	369	0.1	n/n	O
56 (pw63b)	36	7.5	35.5	1700	Hyd. mantle	94	275	369	0.1	n/n	O
57 (pw64b)	38	10	41	1700	Hyd. mantle	94	275	369	0.1	n/n	O

Table 2 (*Continued*)

Model	Plume radius (km)	Age of lithosphere (Ma)	Approx. lithosphere thickness (km)	Temperature of plume (K)	Plume composition	Density contrast lithosphere–plume (kg/m^3)			Plastic strength lithosp. mantle ($\sin(\varphi)$ in Eq. (5))	Mobility melt/fluid	Result[a]
						Thermal (thermal expansion)	Chemical (water, melts, mineralogy)	Total			
58 (pb65)	25	1	13	1700	Hyd. mantle	94	275	369	0.1	y/y	<>
59 (pb66)	24	1	13	1700	Hyd. mantle	94	275	369	0.1	y/y	<>
60 (pb67)	26	1	13	1700	Hyd. mantle	94	275	369	0.1	y/y	<>
61 (pb68)	27	1	13	1700	Hyd. mantle	94	275	369	0.1	y/y	<>
62 (pb69)	70	5	29	1700	Hyd. mantle	94	275	369	0.1	y/y	<>
63 (pb70)	50	2	18.5	1700	Hyd. mantle	94	275	369	0.1	y/y	<>
64 (pt71)	40	10	41	3000	Dry mantle	223	0	223	0.1	y/y	X
65 (pt72)	40	10	41	2500	Dry mantle	173	0	173	0.1	y/y	X
66 (pt73)	40	10	41	2000	Dry mantle	124	0	124	0.1	y/y	X
67 (pt74)	32	5	29	3000	Dry mantle	223	0	223	0.1	y/y	X
68 (pt75)	32	5	29	2500	Dry mantle	173	0	173	0.1	y/y	X
69 (pt76)	32	5	29	2000	Dry mantle	124	0	124	0.1	y/y	X
70 (pt77)	27	2	18.5	3000	Dry mantle	223	0	223	0.1	y/y	X
71 (pt78)	27	2	18.5	2500	Dry mantle	173	0	173	0.1	y/y	X
72 (pt79)	27	2	18.5	2000	Dry mantle	124	0	124	0.1	y/y	X
73 (pt80)	32	5	29	5000	Dry mantle	421	0	421	0.1	y/y	(X)
74 (pt81)	32	5	29	5000	Dry mantle	421	0	421	0.1	y/y	(X)
75 (pr82)	40	3	22.5	1700	Hyd. mantle	94	275	369	0.1	y/y	<> ctbd
76 (pr83)	60	7.5	35.5	1700	Hyd. mantle	94	275	369	0.1	y/y	O
77 (pr84)	20	1	13	1700	Hyd. mantle	94	275	369	0.1	y/y	<>
78 (pr85)	20	2	18.5	1700	Hyd. mantle	94	275	369	0.1	y/y	X
79 (*tc86*)	32	5	*29*	*1850*	*Dry mantle*	109	0	109	0.6[b]	y/y	O

[a] Results of experiments: O = subduction initiation (cf. Fig. 1), X = no subduction initiation (cf. Fig. 2), C = critical subduction initiation (cf. Fig. 3), <> = plate fragmentation (cf. Fig. 4), ctbd = passive counter-bend (cf. Fig. 5c).
[b] Lowering of the lithospheric strength to $\sin(\varphi) = 0.01$ is assumed along the pathways of melt propagation from the plume.

(Gerya and Yuen, 2003b), calculations were performed for each lithology with and without the silicate melt model. Physical properties are computed from these results depending upon whether melt is predicted to be stable from the experimentally constrained phase relations.

2.4. Water migration

Water is both included as free pore-fluid at shallow depths and as a mineralogical component. Initially, the maximal water contents incorporated in hydrous minerals (Table 1) are assigned to the oceanic crust and the thermal–chemical plume, and the rest of the mantle is anhydrous. In addition to water-bearing minerals at low temperature ($T < 600$ K) and pressure ($P < 1.5$ GPa), free water is present in sediments and basaltic crust. Pore water content ($X_{H_2O(p)}$) is assumed to decrease linearly with both P and T as

$$X_{H_2O(p)} = X_{H_2O(p_0)} \left(\frac{600 - T_{(K)}}{327} \right) \times \left(\frac{1.5 - P_{(GPa)}}{1.5} \right), \quad (2)$$

where $X_{H_2O(p0)}$ is the water content at $T = 273$ K and $P = 0.1$ MPa. Here, we conservatively estimate $X_{H_2O(p0)} = 2$ wt.% for both sediments and basaltic crust.

To simulate the migration of water released by dehydration processes, we used independently moving rock and fluid markers (Gorczyk et al., 2007). If water is found to be released in a particular location (i.e., by a particular rock marker), a fluid marker with the respective water amount is generated and moves upwards until it reaches a lithology that assimilates water. Thus, slab dehydration is achieved by setting properties of rock markers to values calculated for stable mineral assemblages, while movement and consumption of generated fluid markers account for water transport. To formulate this method analytically we compute the velocity of fluid markers from the local kinematic transport condition (Gorczyk et al., 2007)

$$v_{x(water)} = v_x, \quad v_{z(water)} = v_z - v_{z(percolation)} \quad (3)$$

where v_x and v_z are local velocity of the mantle and $v_{z(percolation)} = 3$ cm/year is the effective upward percolation velocity of water through the mantle, a pre-assumed constant (Gorczyk et al., 2007).

2.5. Rheological model

The effective creep viscosities of solid rocks are represented as a function of temperature and stress by experimentally determined flow laws (Table 1). Viscosity for dislocation creep depending on strain rate, pressure and temperature is defined in terms of deformation invariants (Ranalli, 1995) as

$$\eta_{creep} = (\dot{\varepsilon}_{II})^{(1-n)/n} F (A_D)^{-1/n} \exp\left(\frac{E + VP}{nRT} \right) \quad (4)$$

where $\dot{\varepsilon}_{II} = \sqrt{(1/2)\dot{\varepsilon}_{ij}\dot{\varepsilon}_{ij}}$ is the second invariant of the strain rate tensor and A_D, E, V and n are experimentally determined flow law parameters (Table 1), respectively material constant, activation energy, activation volume, and stress exponent. F is a dimensionless coefficient that depends on the type of experiments on which the flow law is based and is used for the conversion of experimentally determined rheologies to model stress states. For example:

$F = \dfrac{2^{(1-n)/n}}{3^{(1+n)/2n}}$ for triaxial compression and

$F = 2^{(1-2n)/n}$ for simple shear.

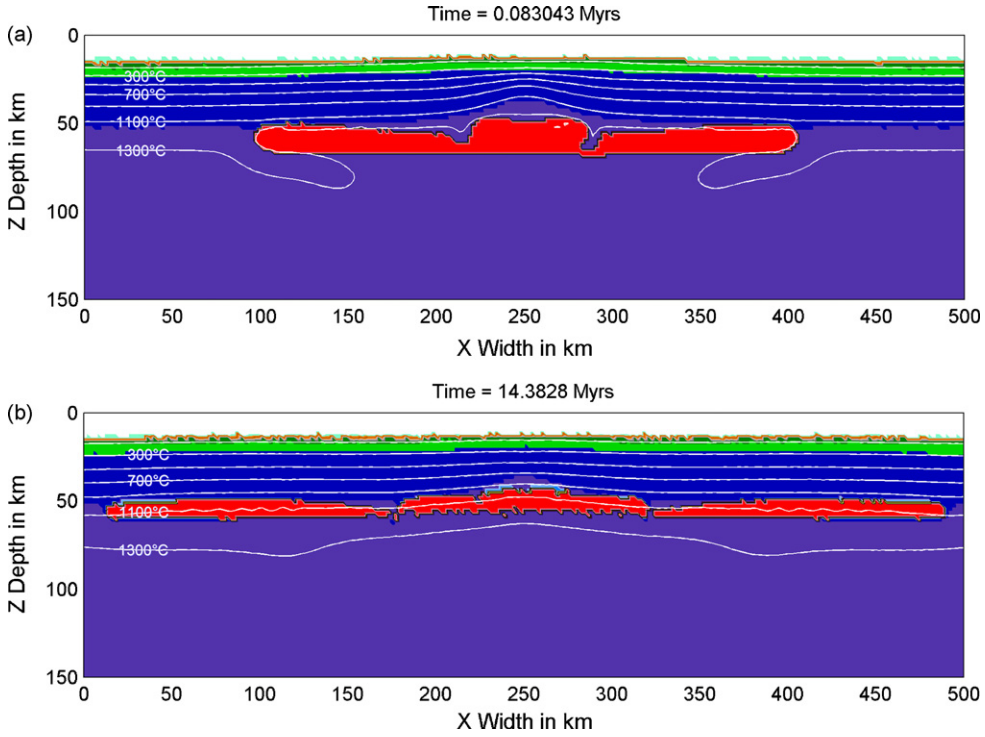

Fig. 2. Failed subduction (model 30). Plume material does not pass through the lithosphere, but continues spreading at the base.

The ductile rheology of solid rocks is combined with a brittle rheology to yield an effective viscoplastic rheology. For this purpose, the Mohr–Coulomb yield criterion (Ranalli, 1995; Byerlee, 1978) is implemented by limiting creep viscosity, η_{creep}, as follows:

$$\eta_{\text{creep}} \leq \frac{c + P\sin(\varphi)}{2\dot{\varepsilon}_{\text{II}}} \tag{5}$$

where c is the cohesion (residual strength at $P = 0$) and φ is the effective internal friction angle (Table 1). We used relatively low values of the initial effective internal friction angle ($0.05 \leq \sin(\varphi) \leq 0.15$) for the whole lithosphere in most of our experiments, implying significant weakening of the lithosphere caused by accumulated fracturing and deep thermal cracking (Korenaga, 2007) and/or fluid and melt activity (e.g., Hall et al., 2003; Sobolev and Babeyko, 2005; Gerya et al., 2008) related to the plume itself. Values significantly lower than those obtained from laboratory experiments have also been proposed by convective system studies (Moresi and Solomatov, 1998; Tackley, 2000; Solomatov, 2004). Following Gerya et al. (2008) we also assume that where the free water fluid is present in the crust or mantle (e.g., due to the slab dehydration), the local effective internal friction angle approaches 0, taking into account that deep sited fluids should have a pressure close to the lithostatic (cf. discussion in Gerya et al., 2008). Similarly, weakening above the partially molten plume is expected due to upward migration of extracted melts.

All partially molten rocks are assigned to a reduced effective viscosity of 10^{17} Pa s (Pinkerton and Stevenson, 1992), which provides a large viscosity contrast with the surrounding dry mantle ($10^{19} - 10^{26}$ Pa s).

2.6. Governing equations and numerical implementation

The momentum, continuity, and thermal equations for the two-dimensional creeping-flow, accounting for thermal and chemical buoyancy, are solved using the modified I2VIS code (Gerya and Yuen, 2003a) based on conservative finite differences and a non-diffusive marker-in-cell technique. The conservation of mass is approximated by the incompressible continuity equation:

$$\frac{\partial v_x}{\partial x} + \frac{\partial v_z}{\partial z} = 0 \tag{6}$$

The 2D Stokes equations take the form:

$$\frac{\partial \sigma_{xx}}{\partial x} + \frac{\partial \sigma_{xz}}{\partial z} = \frac{\partial P}{\partial x} \tag{7}$$

$$\frac{\partial \sigma_{zz}}{\partial z} + \frac{\partial \sigma_{xz}}{\partial x} = \frac{\partial P}{\partial x} - g\rho(T, P, C, M) \tag{8}$$

The density $\rho(T, P, C, M)$ depends explicitly on the temperature (T), the pressure (P), the composition (C), and the mineralogy (M).

The thermal equation is formulated as (Gerya and Yuen, 2003a)

$$\rho C_p \left(\frac{\mathrm{D}T}{\mathrm{D}t}\right) = -\frac{\partial q_x}{\partial x} - \frac{\partial q_z}{\partial z} + H_{\text{r}} + H_{\text{a}} + H_{\text{S}} + H_{\text{L}}, \tag{9}$$

$$q_x = -k(T, C)\frac{\partial T}{\partial x} \quad q_z = -k(T, C)\frac{\partial T}{\partial z}$$

$$H_{\text{a}} = T\alpha\frac{\mathrm{D}P}{\mathrm{D}t} \quad H_{\text{S}} = \sigma_{xx}\dot{\varepsilon}_{xx} + \sigma_{zz}\dot{\varepsilon}_{zz} + 2\sigma_{xz}\dot{\varepsilon}_{xz}$$

where D/Dt is the substantive time derivative; x and z denote, respectively, the horizontal and vertical coordinates; σ_{xx},σ_{xz},σ_{zz} are components of the deviatoric stress tensor; $\dot{\varepsilon}_{xx}$, $\dot{\varepsilon}_{xz}$, $\dot{\varepsilon}_{zz}$ are components of the strain rate tensor; P is pressure; T is temperature; q_x and q_z are heat fluxes; ρ is density; g is the gravitational acceleration; $k(T, C)$ is the thermal conductivity, a function of composition and temperature (Table 1); C_p is the isobaric heat capacity; H_{r}, H_{a}, H_{S}, and H_{L} denote, the radioactive, adiabatic, shear and latent heat production, respectively.

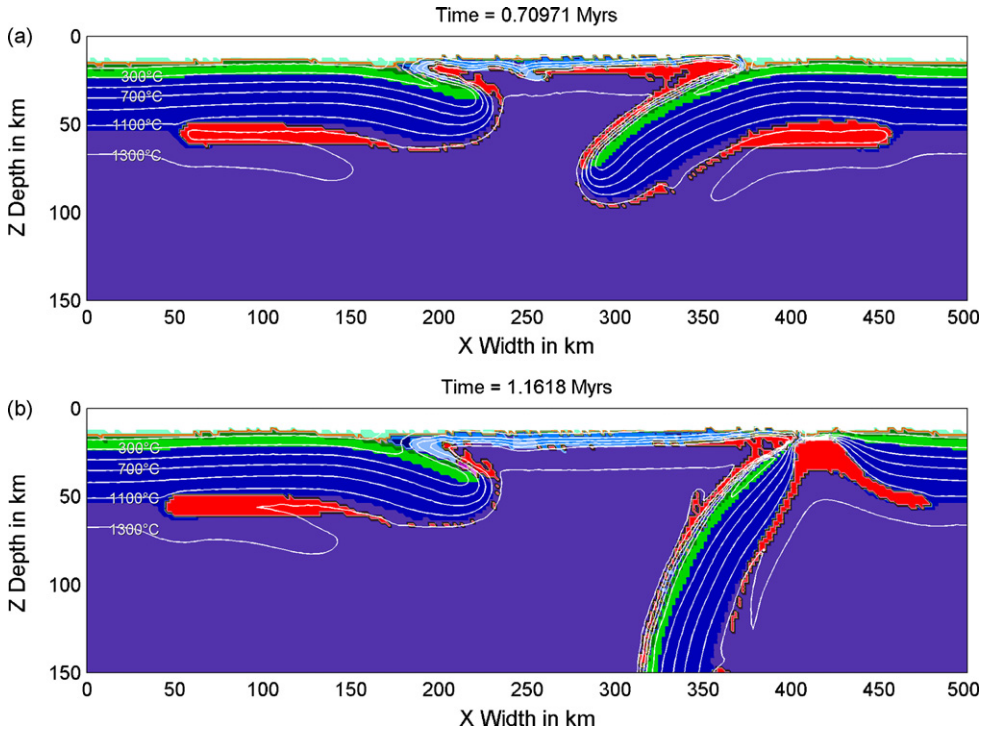

Fig. 3. Asymmetrical or critical initiation (model 2). Only one edge of the disrupted slab subsides and develops into stable subduction.

3. Results

We systematically studied model development in a broad range of physical parameters based on 79 numerical experiments (Table 2). In a certain range of parameters, the impingement of a mantle plume is able to initiate a subduction of relatively thin oceanic lithosphere (Fig. 1). As intended, the buoyant rise of the plume material from the mantle depth leads to the development of a plume structure that spreads when approaching the lithosphere (Fig. 1a and b). In the case of subduction development, the partially molten plume sheet forms a wedge in its middle where material moves upwards through the lithosphere (Fig. 1c). The bulk litho-

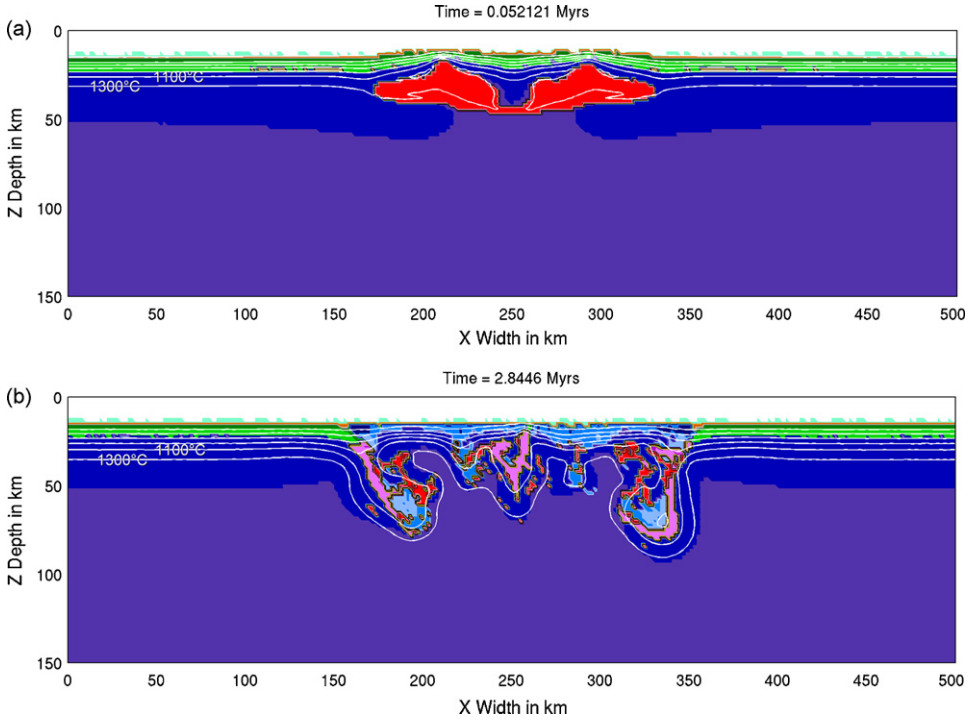

Fig. 4. Overcritical case or slab fragmentation (model 61). Plumes relatively large with respect to lithosphere thickness develop more than one wedge after flattening against the lithosphere and fragment the latter. There are no big fragments that can subduct.

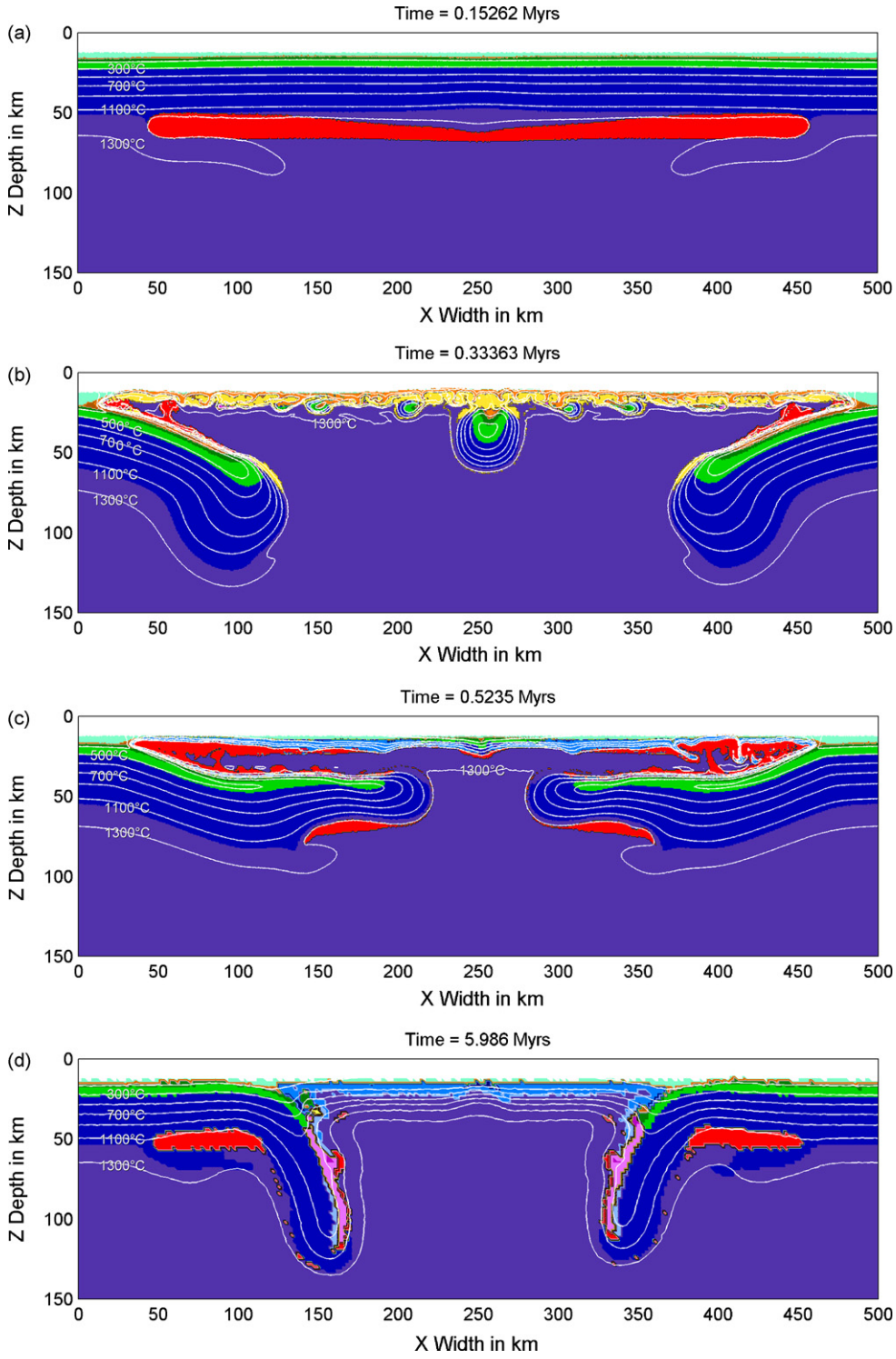

Fig. 5. Influence of various model parameters. (a) Higher lithospheric plastic strength. Plume is not able to pass the lithosphere (model 51). (b) Felsic composition of the plume (model 38). Note the generation of secondary, partially molten peridotite. (c) Lower lithospheric plastic strength (model 46). (d) No fluid release and movement from the slab. Slab movement is dominated by steepening and does not reach comparative depths. Subduction is not self-sustaining and ceases after plume material quenching (model 56). Note the comparatively widely spaced isotherms above and between the slabs.

sphere therefore has a yield strength high enough to force spreading of the plume, but is occasionally overcome by the buoyancy of the latter. The strength is exceeded by the development of a relatively small wedge of partially molten rock centred at the slight bulge over the plume head. This wedge cuts the lithosphere, while portions of the flattened plume remain in their lateral positions at the base of the lithosphere (Fig. 1d). As the wedge portion of the plume, which has a stable and very small width during the transition through the lithosphere, approaches the surface, it spreads again atop of the two created lithosphere segments. This results in a slight initial downward displacement of the plate ends or proto-slabs in order to balance the ascending volume of partially molten plume

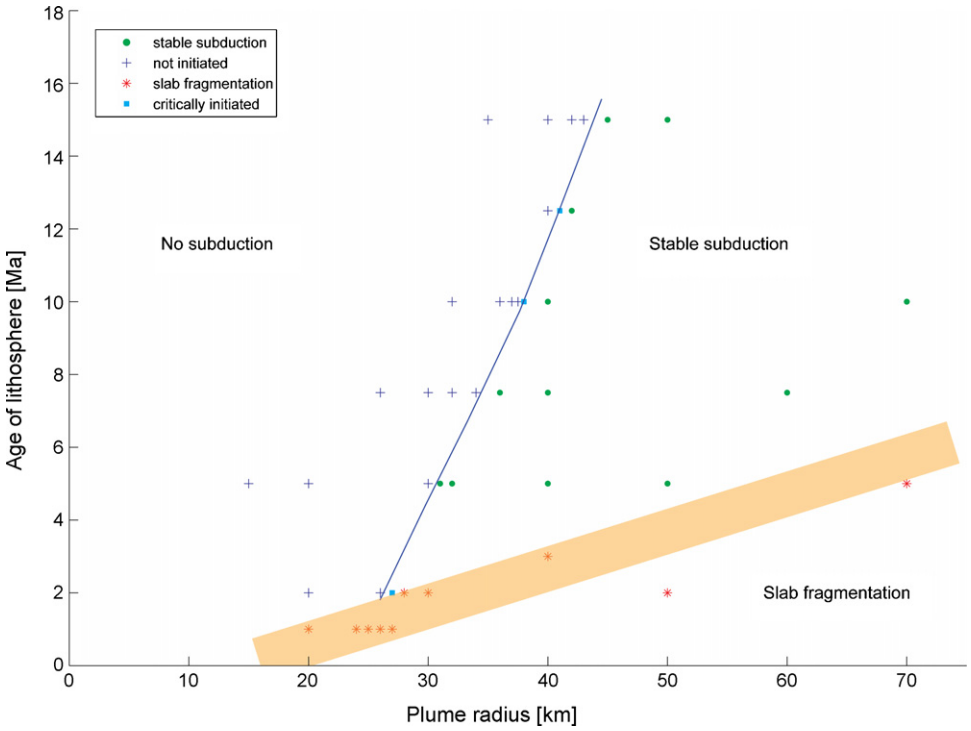

Fig. 6. Summarized regime subdivision. Relations between plume size and the age of the lithosphere appear clearly. However, the behaviour towards slab fragmentation is transitional and can therefore not be located as a sharp line. Plume composition, density and plastic strength of the lithosphere constant for all shown models (hydrated mantle of 3300 kg/m^3, $\sin(\varphi) = 0.1$).

rock (Fig. 1e). The initial downward movement is found to be self-sustaining and to continue as subduction on both sides of the plume (Fig. 1f). After subducting approximately 500 km of lithosphere to depths down to 200 km into the mantle, the slabs detach at shallow depth (Fig. 1g and h), just above the underplating sub-lithospheric, sheet-like remnants of partially molten plume material. Finally, the slabs plunge steeply into the mantle. Related to the formation of a plume material wedge, temporary topographic swell are formed.

Our models show two movement components for the slabs, a retreat of the subduction away from the centre of initiation, but also a steepening of the angle of subduction. Final necking-off and detachment occur at angles of about 50–60°, where the steepening component exceeds the retreating component. Caution is needed in assessing the timescale of the processes investigated. The creation of about 500 km in section of new crust between the retreating slabs occurs in our models within 1 Ma, while the time needed to penetrate through the lithosphere lies in the order of 20,000–50,000 years.

If the choice of plume size is too small, or the lithosphere is chosen to be too old (thus too thick), no subduction occurs (Figs. 2 and 6). The failure of initiation can be observed beginning from an early state, when the flattening of the plume against the lithosphere does not lead to the formation of a topographic swell. No rising wedge of partially molten rocks appears at the centre of the model, and the whole plume material spreads in a symmetrical sheet beneath the lithosphere, apparently resulting in magmatic underplating.

Within a critical range of parameters close to the boundary between these two regimes, a transitional behaviour occurs (cf. critical mode of subduction initiation in Table 1): the initiation of subduction happens asymmetrically with one preferred branch (Fig. 3). The final stage of the shallow slab break-off is, however, reached after the same subduction amount and time as the respective half of a fully developed two-sided system.

On the other hand, when the plume size is large, the resulting interaction with the lithosphere appears more complex (Fig. 4). Post-flattening stages of the plume do not follow a simple wedge formation, rising through lithosphere, and flood-like spreading sequence (which initiates subduction), but rather lead to more complex and multi-fold patterns of plume material uprise, lithosphere fragmentation and balancing counter-movements of partly reworked lithospheric material into shallow mantle depths (Fig. 4b). For large plume size/lithospheric thickness (or age) ratios, a single central wedge of melt does not form to pass the lithosphere, but rather two or possibly more locations of uprise are observed (Fig. 4a). The developing topography, correlative to the degree of lithosphere uplift over the buoyancy push, is much more pronounced than in the stable case, and displays steeper angles between plume flow and proto-slabs. These cases lead to smaller lithospheric fragments that do not subduct or that stack and are resorbed in the mantle early. If additionally the lithosphere is very young (or hot; e.g., model 63), down-warp of proto-slabs by plume material is not rigidly transmitted; they instead flatten at very shallow levels, as described below for cases with lowered plastic strength. However, the transition from stable, retreating subduction to slab fragmentation is not sharp, but occurs over a range of initial parameters, reflected in the early separation of a central melt wedge into two wedges, subsequently migrating away from the centre, as the ratio of plume size/lithospheric age increases. We have chosen these criteria of wedge-splitting and the directly related fragmentation of the lithosphere to classify the corresponding models into a regime that is denoted as slab fragmentation.

The variation of other initial parameters (Fig. 5) has shown that the effect of plume composition is larger than the effect of plume temperature. Temperatures required to overcome the tested low lithospheric plastic strength ($\sin(\varphi) = 0.1$) with a purely thermal plume (i.e., when density reduction due to the hydration and melt-

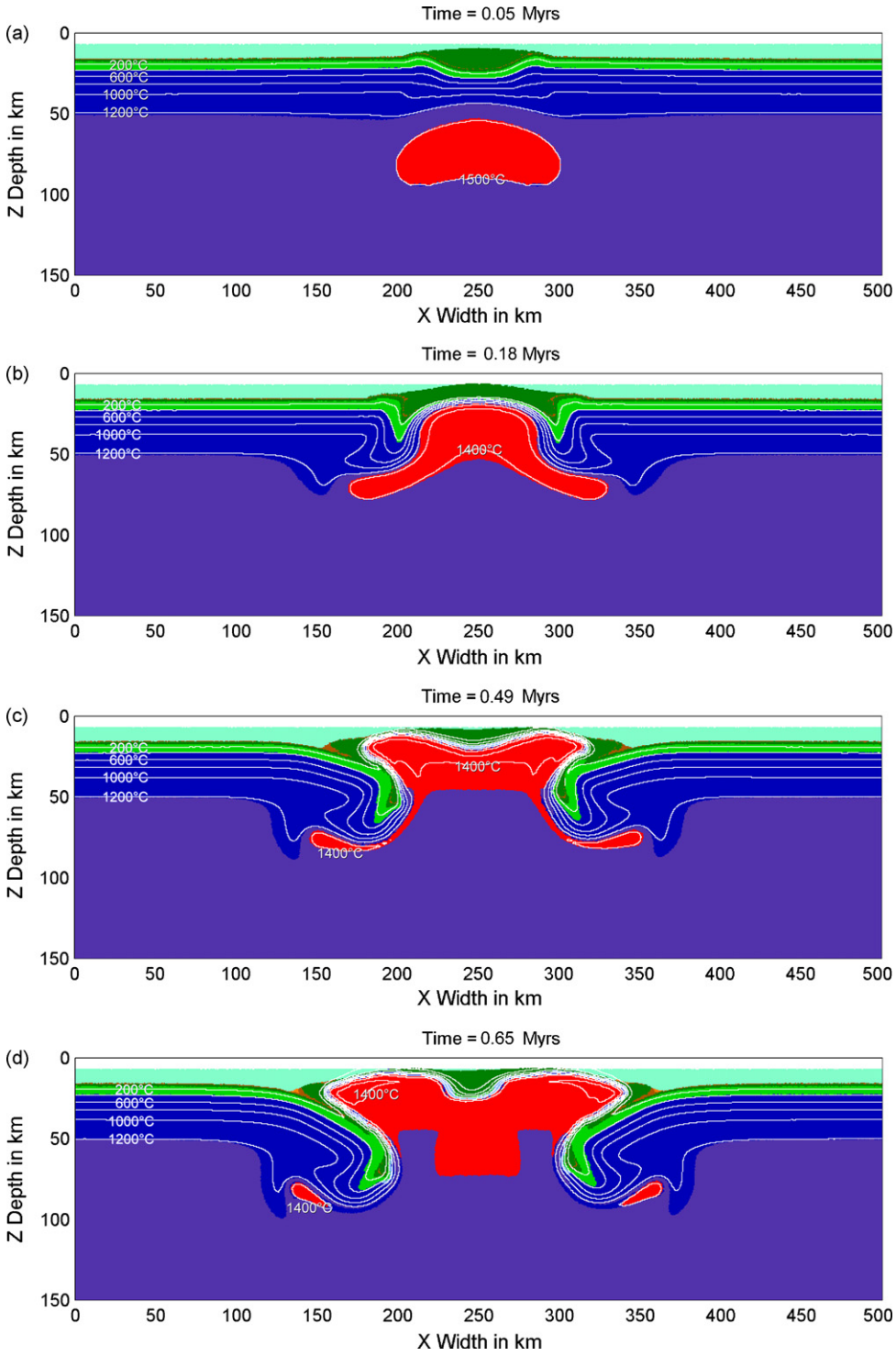

Fig. 7. Initiation of subduction of strong ($\sin(\varphi) = 0.6$) thin/young (5 Ma) lithosphere by partially molten thermal ($\Delta T = 300$ K) plume composed of dry ambient mantle (model 79). Lowering of the lithospheric strength to $\sin(\varphi) = 0.01$ is assumed along the pathways of melt propagation from the plume. New mafic crust (cf. thick dark green layer) above the plume is formed due to the melt extraction, which limits increase in plume buoyancy during the decompression melting. See text for discussion. (For interpretation of the references to colour in this figure legend, the reader is referred to the web version of the article.)

ing is not considered) lie widely beyond the reasonable range, at about 5000 K.

In contrast, the variation of the plume's composition highlighted the strong influence of the chemical component of density (Table 2). We have described the different plume–lithosphere interactions for a plume of hydrous mantle composition in the sections above. Moderately buoyant plumes with mafic composition (density contrast with the lithosphere = 165 kg/m^3, initial water content = 2.8 wt.%; see mafic lithology in Table 1) failed to reach the critical post-flattening stages and only underplated the lithosphere. Tests with felsic plumes (density contrast 800 kg/m^3, initial water content = 7.6 wt.%; see felsic lithology in Table 1) lead to even faster lithosphere penetration and subduction initiation (Fig. 5b). With the given high density contrast and hydration, the plume does not

stagnate first (cf. Fig. 1b) at the base of the lithosphere, but flattens during ongoing ascent up to the surface. These models can develop two centres of post-flattening ascent and still initiate subduction successfully. Between the centres of ascent a small immobile piece of lithosphere remains entrapped in the central part of the models (Fig. 5b).

We also tested a possible influence of slab strength by varying the internal friction angle of the entire lithosphere while keeping most other parameters constant, slightly varying plume size for a given friction angle. If raised ($\sin(\varphi) = 0.15$), no penetration of plume through the lithosphere has been observed (Fig. 5a), resulting in a tectonic structure similar to those for failed plumes due to low plume size/lithosphere age ratios (Fig. 2). If lowered ($\sin(\varphi) = 0.05$), surficial spreading/flooding of a passed plume portion did not result in a stable downshift with subsequent, self-sustaining subduction (Fig. 5c). Instead, the initial foundering of slab ends stagnated in shallow depths, and the slabs re-adjusted to a horizontal orientation behind the advancing process zone at the tips of the spreading plume material (passive counter-bend). The result (Fig. 5c) is a horizontal density stratification with over-solidus mantle overlaying colder lithosphere.

Final parameter testing has addressed the issue of fluid release and circulation. We have disabled the propagation of volatiles (water, but also melt) as a free phase in some models (cf. Table 2) and compared the resulting interaction schemes with parallel cases featuring identical initial parameterization, but with suppressed fluid propagation. The stagnant-fluid models are characterized by breaking of the lithosphere, an initial subduction initiation, fast steepening of subduction angle, stagnating position (no retreat), and stacking and resorption of the almost vertical plunging slabs in shallow mantle depths (Fig. 5d). Isotherms are more widely spaced between and above the plume compared to similar models with mobile volatiles.

4. Discussion

4.1. Interpretation of results

The possibility to initiate self-sustaining, retreating subduction as a result of a plume event is limited to a certain parameters range in our models. Differences in initial parameters were able to create a spectrum of resulting plume–lithosphere interactions, in which three major regimes can be recognized: (1) failure of complete rise and magmatic underplating; (2) passing of partially molten plume material through the lithosphere and initiation of retreating subduction; (3) massive or multiple passing of plume material and fragmentation of the lithosphere into pieces which are eventually resorbed. We have termed these regimes *failure*, *initiation*, and *fragmentation*, and have found that they correspond to relatively well-constrained fields in a plot of plume size versus lithospheric age (or lithospheric thickness) (Fig. 6). However, the change of interaction behaviour from stable subduction to fragmentation appears rather broad and transitional; on the other hand, critical cases of subduction initiation, with only one side developed, lie well in proximity to the best-fit boundary line between failure and subduction. We have chosen to locate the boundaries between the regimes in Fig. 6 with a corresponding breadth.

4.1.1. Geometry and stresses

The development of self-sustaining, retreating subduction seems to depend on some critical stages. After buoyancy-driven ascent and lowering of plume density owing the decompression melting, the flattening plume needs to develop one central wedge (Fig. 1c) that is able to rise upwards through the lithosphere, overcoming the lithospheric cohesion. The spreading of passed plume rocks atop the proto-slabs (Fig. 1d) and overriding them, is important to deliver an initial downwards forcing. Vertical stress results from isostasy and magmatic loading. Horizontally, there is local compression at the tips of the propagating "melt bubble", and extension between tips and the centre of the model. This mechanism for the triggering of slab foundering is very similar to that proposed by Kemp and Stevenson (1996) for a passive margin under extension, but here extended to bi-directional spreading of the mantle material. Gravitational loading (mantle) provides the initial downshift in both studies; in comparison, however, our plume scenario requires neither predefined inhomogeneities in the lithosphere (ocean–continent transition) nor external tension.

While the role of the spreading plume rocks is easily understood as a buoyant displacement, the reason for the importance of the geometric centring of melt uprise remains less clear. Should two wedges develop instead (Fig. 4a), they interfere, either by developing counteracting horizontal forces similar to ridge-pushes to the centre, or by being part of small-scale convection cells (Solomatov, 2004) in the uppermost mantle. In addition, related steeper contact angles between the wedge of partially molten material and proto-slab as simultaneously plume radius increases might make the magmatic loading increasingly inefficient. In fact, some of these models (e.g., model 61) display small-scale (spanning $10 < z < 75$ km) convection cells including the slabs, while in one-wedge cases no or far less convection appears. Material flow seems to be mainly limited to separate layers below and above the slab. In the few models with excess buoyancy (felsic plumes), two centres of melt ascent can also initiate subduction, and oppositely directed stable stresses trap a small piece of lithosphere under compression in the centre.

4.1.2. Buoyancy

As we have seen above, the critical condition to trigger subduction by mantle plume is that it should be able to pass through the entire lithosphere. This may happen only if the plume buoyancy exceeds the local strength of the lithosphere. The dominance of compositional over thermal buoyancy for various plumes tested in our experiments is visible in Table 2. Plumes of wet mantle composition (Table 2) are buoyant enough to trigger break-up, but are close to critical in the parameter range (primarily internal friction angle φ of the lithosphere) we have investigated here. Mafic plumes (Table 2) are initially slightly less buoyant due to the presence of dense iron-bearing garnet and failed to break the lithosphere within the limited extent of our investigation, it seems therefore that a required density contrast exists which should be about or over 300 kg/m^3 (summing both thermal and compositional buoyancy) for our experiments with $\sin(\varphi) = 0.1$. Strongly compositionally buoyant felsic plumes (Table 2) also contain significantly more water and melts leading to faster lithosphere penetration and subduction initiation (Fig. 5b). Pure thermal plumes (Table 2) showed accordingly low potential for breaking the lithosphere.

Changing buoyancy has yet another important implication for our models. As proto-slabs are down-warped in the mantle, they can reach depths of major mineralogical changes. Dehydration, and especially the transition of the gabbroic portions of the lithosphere to eclogite (Ahrens and Schubert, 1975), increase the density of the lithosphere and make it negatively buoyant, which will start to create a downward pull. Thus, forced temporary dipping of the slabs in mantle depths (varying on thermal conditions; e.g., Peacock and Wang, 1999) for which they would be too buoyant can create forces that make foundering of slabs self-sustaining and stabilize subduction.

4.1.3. Plastic strength

Considering that in the upper cold part of the lithosphere the deformation is dominated by friction plasticity, we obtain that the condition for the plume to pass through is

$$\Delta\rho g R > a \sin(\varphi)\rho g H \quad (10)$$

where R is plume radius, $\Delta\rho$ is its total density deficit relative to the surrounding lithosphere, φ, is friction angle of the lithospheric material above the plume, ρ is density of the lithosphere, H is its thickness and a is a coefficient, which is of the order of unity.

With the parameters used in most of our experiments the above simple relation describes well the subduction initiation domain in Fig. 6 if coefficient a is 0.7–0.8 (H = 35–50 km, R = 30–45 km, $\sin(\varphi) = 0.1$, $\Delta\rho = 300\,\mathrm{kg/m^3}$, $\rho = 3300\,\mathrm{kg/m^3}$).

If the plume radius and buoyancy, as well as lithospheric thickness and density are fixed, Eq. (10) gives the critical lithospheric strength (critical friction angle)

$$\sin(\varphi)_{\mathrm{critical}} = \frac{\Delta\rho R}{a\rho H}, \quad (11)$$

If the friction angle of the lithosphere above the plume is lowered to the values below the critical, the plume can penetrate the lithosphere and initiate subduction; otherwise, it cannot.

From Eq. (11) it is clear why a purely thermal plume failed to initiate subduction in some of our experiments. The reason is that, with relatively small buoyancy of the purely thermal plume (compared to the buoyancy of thermo-chemical plume), the lithospheric strength above the plume assumed in the experiments ($\sin(\varphi) = 0.1$) appeared to be much higher than critical. According to Eq. (11) the effective friction coefficient of the lithosphere must be lowered to the value of about 0.01 to initiate subduction above the thermal mantle plume with an excess temperature of 300 °C. We have checked this estimate with an additional numerical experiment (Fig. 7, model 79). In this experiment, we assumed an initially strong lithosphere ($\sin(\varphi) = 0.6$) hit by a thermal plume composed of ambient dry mantle subjected to partial melting during the decompression. The melt fraction in the plume is kept relatively low (2–4 vol.%) due to the assumed intense melt extraction. Extracted melts propagate upwards (we modelled instantaneous kinematic melt propagation) across the lithosphere and are deposited on top of it in the form of new basaltic crust (note thick dark green layer forming above the plume in Fig. 7a and b). The plastic strength of the lithosphere along melt propagation pathways (Korenaga and Kelemen, 1998) is lowered to $\sin(\varphi) = 0.01$. As we see from Fig. 7, this model based on strong magmatic weakening of the lithosphere strictly above the areas of melt extraction from the plume is able to initiate subduction. Our expectation about the critical degree of plastic strength lowering appears to be correct. In contrast to numerical experiments with low plastic strength for the entire lithosphere (Fig. 1), in the model with globally strong but locally weakened plates, final detachment of the slabs does not occur and paired retreating subduction continues in a self-sustaining way.

Therefore, our experiments demonstrate that, in 2D-geometry, a mantle plume can break the lithosphere and initiate self-sustaining subduction if it causes intensive enough (critical) local weakening of the lithospheric material above it. The required weakening depends on the plume volume, plume buoyancy and thickness of the lithosphere. The required friction drop is the largest (effective friction coefficient drop from 0.5–0.7 to about 0.01) for the least buoyant purely thermal plumes and it is less dramatic (from 0.5–0.7 to about 0.1) for the strongly buoyant thermo-chemical plumes.

We note that effective friction coefficients of 0.1 and especially 0.01 are much lower than laboratory-measured values for the typical dry lithospheric materials (0.5–0.7; Byerlee, 1978). However, low local friction coefficients are thought to be typical for large active transform faults like the San Andreas Fault (Zoback et al., 1987; Bird and Kong, 1994) and especially for material of a subduction channel, decoupling subducting and overriding plates (Sobolev and Babeyko, 2005), where effective friction of rocks is drastically lowered by the high-pressure fluids. Values up to one order of magnitude lower than laboratory values have also been postulated (Moresi and Solomatov, 1998; Tackley, 2000; Solomatov, 2004) for the bulk oceanic lithosphere due to various weakening mechanisms. On the other hand, it has been recently demonstrated by Gerya et al. (2008) that self-sustaining, one-sided subduction characteristic for the present-day Earth requires strong plates locally weakened by fluid and melt activities—a condition that we tested with globally strong but locally weakened plates (Fig. 7). That means that the presence of high-pressure volatiles (melts or fluids) coming from the plume and lowering material effective friction coefficient in the lithosphere above the plume is a crucial condition for the plume to penetrate the lithosphere and to initiate subduction. Initial break-up can either occur with a locally strong dynamic weakening due to melts and volatiles, or equally with a pre-defined, moderately weakened lithosphere on a global scale. Lowering the strength globally can however have major consequences on the behaviour of the slabs during earliest subduction stages because, as demonstrated, an internal friction coefficient of 0.05 does not lead to stable subduction in our models.

4.1.4. Volatiles

As it is demonstrated by our experiment without water in the slab, when the subduction failed shortly after the initiation, a critical issue for self-sustaining subduction is the presence of the high-pressure fluids at the slab upper interface, in accordance with previous results (e.g., Sobolev and Babeyko, 2005; Gerya et al., 2008). Water is able to lower the angle of internal friction significantly when forming a new plate boundary. Later, the lubrication (Lenardic and Kaula, 1994) can lower the friction at the slab surface when subducting along this boundary. Water therefore exerts a strong control on the decoupling (Gerya et al., 2008) of one plate fragment from the other and from the adjacent material (here, overlaying mantle). Finally, if slabs dehydrate in the upper mantle, their density will increase, additionally facilitating downward movement. The importance of volatiles in our study is in good agreement with the conclusion of Regenauer-Lieb et al. (2001) that lithosphere can only break along its entire thickness along a sharp new boundary if lubrication is provided. Our observation is also in agreement with the model for long-term subduction cycles (Van der Lee et al., 2008) where slab-derived volatiles in the underlying mantle from an earlier subduction episode or from an opposing margin of the same continent provide the critical weakening of the lithosphere at a passive margin. The plume model has in this context directly been proposed (Van der Lee et al., 2008) as the initial triggering mechanism for subduction in the Archean.

In summary, subduction may be initiated when the lithosphere is locally broken and lubricated slabs of moderately dense lithosphere reach critical mantle depths because of a downshift when being overridden by lighter, hot plume material. At these depths, densification due to phase changes can create a downward drag at the slab tip and make subduction self-sustaining. To reach these depths, it seems to be necessary that slabs can be deflected a bit further down after reaching their density equilibrium in the mantle by rigidly transmitted downshift at the process zone of the trench. Further, we conclude that in order to initiate subduction, the plume must be (i) strongly buoyant and large, but even more importantly, it must (ii) be able to lower drastically the effective friction coefficient in the lithosphere above it. The way to do that is to generate a large volume of high-pressure fluids and/or melts penetrating the lithosphere. Finally, even if subduction is initiated it becomes

self-sustaining only if the fluids severely decrease friction at the interface between the slab and overlying mantle portion.

Interestingly, our experiments show that even rather young (thin), positively buoyant lithosphere (Cloetingh et al., 1989) can have a self-sustaining subduction mode if the conditions of subduction initiation by plume, mentioned above, are fulfilled. That is in apparent contradiction with the suggestion (Cloos, 1993) that only lithosphere older than around 10 myears that is negatively buoyant in the mantle can be subducted. The reason for this contradiction is that in our modelling, we include a gabbro-eclogite transformation. When the plume initiates subduction, the slab edge subsides to several tens of kilometres, where gabbro turns to eclogite, increasing density of the oceanic crust (Ahrens and Schubert, 1975) and making even very thin (young) oceanic lithosphere negatively buoyant. One important consequence of this effect for our modelling is that even in the case of thicker (i.e., >7 km) proto-oceanic crust, a relatively thin lithosphere will be able to subduct if penetrated by the mantle plume. Although we have built our models on some major assumptions (that is, a fluid-rich, relatively hot plume, negligence of elasticity, and homogeneity in the third dimension), plumes have conceptually shown to have a significant potential for both rupturing the lithosphere and for triggering its foundering. Moreover, in contrast to other models, our model does not require any external forces (Kemp and Stevenson, 1996; Han and Gurnis, 1999; Hall et al., 2003) or inhomogeneities of the lithosphere (McKenzie, 1977; Mueller and Phillips, 1991; Toth and Gurnis, 1998; Hall et al., 2003), also meaning that it can initiate subduction anywhere plumes hit within the oceanic lithosphere. Further validation of this concept will require quantitative studies in three dimensions.

4.2. Possible analogues

4.2.1. Applicability to present-day Earth

This study has modelled the hypothetical initiation of subduction as a result of a plume in two dimensions. We have outlined the limitations and the justification for this assumption in the introduction. Given the very high speed and relatively short duration (1 Myr) of the corresponding processes, the results from numerical experiments with globally weak lithosphere (Fig. 1) seem not to be applicable to present-day Earth and are not matched by geological observations. However, if some assumptions, the model setup and a number of parameters were changed, the resulting subduction might start under more realistic conditions (e.g., by assuming globally strong but locally weakened plates, Fig. 7). For example, increasing bending strength and limiting energy dissipation by incorporating elasticity into modelled rheologies (Funiciello et al., 2003) could lead to different foundering behaviour and may stabilize subduction further; similarly, superimposed far-field compression would reduce the amount of retreat, would allow a more elevated "melt bubble" and more efficient loading, and would thus allow for easier initiation of subduction. The major limitation seems to be the need for a comparatively small but strongly buoyant plume, preferably with some water content; one could think of plumes originating from the transition zone between 410 and 660 km and incorporating water from stagnating thermally relaxing slabs (Richard et al., 2006) which would make them compositionally (but not thermally) buoyant. Such a plume would then need to hit a small plate fragment like those of the Juan de Fuca plate. We think that, although apparently not realized, plume-induced subduction could theoretically initiate on present-day Earth, provided that certain uncommon circumstances coincide.

4.2.2. Earlier Earth—Archean

In contrast, higher heat flux and steeper thermal gradients are postulated for the Archean lithosphere. Higher mantle temperature should result in wide-spread/global presence of partially molten regions below the lithosphere, which could in turn result in the globally weaker plates affected by propagation of extracting melts. Although we cannot consider our models with globally weak plates as a direct thermal analogue to the earlier Earth, we might have sketched some possible interactions in constructing our three proposed regimes. It should have been easier for a plume to pass through a thin, hot lithosphere. In addition, there is a strong argument that Archean plumes were comparatively enriched in water (cf. Grove and Parman, 2004, and references therein), and therefore, could have contained large volumes of melt. Leaving aside the success or failure of initiation, small subcritical plumes could have contributed to local underplating (our failure mode). Furthermore, our fragmentation mode might correspond to late Archean crustal reworking (Rey et al., 2003). Considering the initiation and slab fragmentation modes, our results show that different tectonic settings can develop from only gently varied parameters. Applied to the controversial development of ultramafic komatiites (Grove and Parman, 2004), geochemically different komatiites with characteristics of a plume or subduction zone origin might have developed from rather similar starting points, and the two creation mechanisms may have co-existed. Plume-triggering of subduction provides in principle a simple mechanism to start for the first time a system of subduction tectonics that can reconfigure (Stern, 2004) and may remain active for hundreds of Ma (Van der Lee et al., 2008) or even until the present.

4.2.3. Venus coronae (3D)

We have so far discussed implications derived from the 2D-experiments and assumed homogeneity in the third dimension. In a similar model setup in three dimensions assuming a cylindrical plume and an intact oceanic lithosphere at the beginning, stresses and mechanisms should act equally in all horizontal directions after impingement and plume material ascent. This would imply that the developing subduction zone would have the shape of a ring or funnel. This must be treated with some caution because the interaction between resulting stresses and movements in different directions around the ring would have to be taken into account and might partly counteract, leading to a much stiffer "slab" structure. Subduction could still be possible if (lateral) movement would take place not all at once, but rather sequentially in different portions of the structure (Sandwell and Schubert, 1992).

There are indeed reports of tectonic structures for which a ring-shaped (partial) subduction might represent a good model, namely circular structures on Venus that have been subject to different interpretations in the past (Grindrod et al., 2006; Hansen, 2003, 2006; Krasil'nikov et al., 2001; Hoogenboom and Houseman, 2006). Fowler and O-Brien (1996) have, in an analytical study, proposed that coronae as subduction rims formed above a plume, assuming that the latter did not emerge through the lithosphere. Earlier, Sandwell and Schubert (1992) had, based on striking similarities between topographic profiles over the rim of bigger Venus coroane and over Earth trenches, suggested that these corona rims were also signs of retreating subduction. In fact, Sandwell and Schubert (1992) have also suggested a (fully ascending) plume origin for these structures, with the very same mechanisms of subduction development as those described in this paper. Here, we were able to reproduce and confirm their proposal with a dynamic model that is strikingly similar in section (cf. their Fig. 6). Based on our results, we expect that peripheral subduction on Venus would not be stable, and would correspond to the fast steepening and freezing scenarios (Fig. 5d) when slab dehydration was not allowed in the models. This is in accordance with the commonly assumed absence of water in the Venus mantle and crust. However, taking into account that subducting slabs in such a case do not retreat, and should be quite

rare, it is likely that subduction did not contribute much to the resurfacing of Venus (Turcotte et al., 1999; Reese et al., 1999).

5. Conclusion

2D modelling has successfully been used to test mantle plumes as a possible trigger of retreating oceanic subduction. Interaction with the lithosphere exhibits three distinct plume size/lithospheric age regimes, but is not fully constrained with respect to numerous other parameters. Qualitatively, the importance of a compositionally buoyant plume, free volatiles, and volatile-induced lowering of the plastic strength of the lithosphere above the plume has been shown. We have hereby presented an interesting possibility to initiate subduction self-consistently without the need for external plate forces, pre-included inhomogeneities, or global weakening of the lithosphere.

Acknowledgements

We would like to thank W. Gorczyk for provision of visualization routines and basic instructions and J.-P. Burg and P. Tackley for supporting the realization of the project. The manuscript profited enormously from helpful suggestions and review by Slava Solomatov and an anonymous reviewer. This work was supported by ETH Research Grants TH-12/05-3, TH-08/07-3 and SNF Research Grant 200021-113672/1 to TVG.

References

Ahrens, T.J., Schubert, G., 1975. Rapid formation of eclogite in a slightly wet mantle. Earth Planet. Sci. Lett. 36, 43–46.
Byerlee, J., 1978. Friction of rocks. Pure Appl. Geophys. 116, 615–626.
Bird, P., Kong, X., 1994. Computer simulations of California tectonics confirm very low strength of major faults. Geol. Soc. Am. Bull. 106, 159–174.
Branlund, J.M., Regenauer Lieb, K., Yuen, D.A., 2001. Weak zone formation for initiating subduction from thermo-mechanical feedback of low-temperature plasticity. Earth Planet. Sci. Lett. 190, 237–250.
Brown, M., 2006. Duality of thermal regimes is the distinctive characteristic of plate tectonics since the Neoarchean. Geology 34, 961–964.
Brown, M., 2007. Metamorphic conditions in orogenic belts: a record of secular change. Int. Geol. Rev. 49, 193–234.
Burg, J.P., Gerya, T.V., 2005. The role of viscous heating in Barrovian metamorphism of collisional orogens: thermomechanical models and application to the Lepontine Dome in the Central Alps. J. Metamorph. Geol. 23, 75–95.
Burov, E., Guillou-Frottier, L., 2005. The plume head-continental lithosphere interaction using a tectonically realistic formulation for the lithosphere. Geophys. J. Int. 161, 469–490.
Clauser, C., Huenges, E., 1995.Thermal conductivity of rocks and minerals. In: Ahrens, T.J. (Ed.), Rock physics & phase relations: a handbook of physical constants. AGU reference shelf, vol. 3, pp. 105–126.
Cloetingh, S., Wortel, R., Vlaar, N.J., 1989. On the initiation of subduction zones. Pure Appl. Geophys. 129, 7–25.
Cloos, M., 1993. Lithospheric buoyancy and collisional orogenesis: subduction of oceanic plateaus, continental margins, island arcs, spreading ridges, and seamounts. Geol. Soc. Am. Bull. 105, 715–737.
Connolly, J.A.D., Petrini, K., 2002. An automated strategy for calculation of phase diagram sections and retrieval of rock properties as a function of physical conditions. J. Metamorph. Geol. 20, 697–708.
d'Acremont, E., Leroy, S., Burov, E., 2003. Numerical modelling of a mantle plume: the plume head-lithosphere interaction in the formation of an oceanic large igneous province. Earth Planet. Sci. Lett. 206, 379–396.
Fowler, A.C., 1993. Boundary layer theory and subduction. J. Geophys. Res. 98, 21997–22005.
Fowler, A.C., O-Brien, S.B.G., 1996. A mechanism for episodic subduction on Venus. J. Geophys. Res. 101, 4755–4763.
Funiciello, F., Morra, G., Regenauer-Lieb, K., Giardini, D., 2003. Dynamics of retreating slabs: 1. Insights from two-dimensional numerical experiments. J. Geophys. Res. 108, 2206.
Gerya, T.V., Connolly, J.A.D., Yuen, D.A., 2008. Why is terrestrial subduction one-sided? Geology 36, 43–46.
Gerya, T.V., Connolly, J.A.D., Yuen, D.A., Gorczyk, W., Capel, A.M., 2006. Seismic implications of mantle wedge plumes. Phys. Earth Planet. Inter. 156, 59–74.
Gerya, T.V., Yuen, D.A., 2003a. Characteristics-based marker-in-cell method with conservative finite-differences schemes for modeling geological flows with strongly variable transport properties. Phys. Earth Planet. Inter. 140, 295–320.
Gerya, T.V., Yuen, D.A., 2003b. Rayleigh–Taylor instabilities from hydration and melting propel 'cold plumes' at subduction zones. Earth Planet. Sci. Lett. 212, 47–62.
Gerya, T.V., Perchuk, L.L., Maresch, W.V., Willner, A.P., 2004. Inherent gravitational instability of hot continental crust: implication for doming and diapirism in granulite facies terrains. In: Whitney, D., Teyssier, C., Siddoway, C.S. (Eds.), Gneiss Domes in Orogeny. GSA Special Paper, vol. 380, pp. 97–115.
Ghiorso, M.S., Hirschmann, M.M., Reiners, P.W., Kress, V.C., 2002. The pMELTS: a revision of MELTS for improved calculation of phase relations and major element partitioning related to partial melting of the mantle to 3 GPa. Geochem. Geophys. Geosyst., 3: art. no.-1030.
Gorczyk, W., Willner, A.P., Connolly, J.A.D., Burg, J.-P., 2007. Physical controls of magmatic productivity at Pacific-type convergent margins: new insights from numerical modeling. Phys. Earth Planet. Inter. 163, 209–232.
Griffin, W., O'Reilly, S., Abe, N., Doyle, B., Kivi, K., 2003. The origin and evolution of Archean lithospheric mantle. Precambrian Res. 127, 19–41.
Grindrod, P.M., Stofan, E.R., Brian, A.W., Guest, J.E., 2006. The geological evolution of Altai Mons, Venus: a volcano-corona 'hybrid'. J. Geol. Soc. Lond. 163, 265–275.
Grove, T.L., Parman, S.W., 2004. Thermal evolution of the Earth as recorded by komatiites. Earth Planet. Sci. Lett. 219, 173–187.
Gurnis, M., Hager, B.H., 1988. Controls of the structure of subducted slabs. Nature 335, 317–321.
Gurnis, M., Hall, C., Lavier, L., 2004. Evolving force balance during incipient subduction. Geochem. Geophys. Geosyst. 5, art-no. 00681.
Hall, C.E., Gurnis, M., Sdrolias, M., Lavier, L., Müller, R., 2003. Catastrophic initiation of subduction following forced convergence across fracture zones. Earth Planet. Sci. Lett. 212, 15–30.
Han, L., Gurnis, M., 1999. How valid are dynamic models of subduction and convection when plate motions are prescribed? Phys. Earth Planet. Inter. 110, 235–246.
Hansen, V.L., 2003. Venus diapirs: thermal or compositional? Geol. Soc. Am. Bull. 115, 1040–1052.
Hansen, V.L., 2006. Geologic constraints on crustal plateau surface histories, Venus: the lava pond and bolide impact hypothesis. J. Geophys. Res. 111, E11010.
Hoogenboom, T., Houseman, G.A., 2006. Rayleigh–Taylor instability as a mechanism for corona formation on Venus. Icarus 180, 292–307.
Ismail-Zadeh, A., Schubert, G., Tsepelev, I., Korotkii, A., 2006. Three-dimensional forward and backward numerical modeling of mantle plume evolution: effects of thermal diffusion. J. Geophys. Res. 111, B06401.
Kaus, B.J.P., Podlachikov, Y.Y., 2001. Forward and reverse modeling of the three-dimensional viscous Rayleigh–Taylor instability. Geophys. Res. Lett. 28, 11095–11098.
Kemp, D.V., Stevenson, D.J., 1996. A tensile, flexural model for the initiation of subduction. Geophys. J. Int. 125, 73–94.
Kerrick, D.M., Connolly, J.A.D., 2002. Quantification of subduction zone metamorphic devolatilization from computed high pressure phase equilibria. Geochim. Cosmochim. Acta 66, A396.
Korenaga, J., Kelemen, P.B., 1998. Melt migration through the oceanic lower crust; a constraint from melt percolation modelling with finite solid diffusion. Earth Planet. Sci. Lett. 156, 1–11.
Korenaga, J., 2007. Thermal cracking and the deep hydration of oceanic lithosphere; a key to the generation of plate tectonics? J. Geophys. Res. 112, 05408.
Krasil'nikov, A.S., Galkin, V.A., Basilevsky, A.T., 2001. Tectonics and evolution of Coronae on Venus: preliminary results of tectonophysical modeling. Solar Syst. Res. 35, 103–116.
Lenardic, A., Kaula, W.M., 1994. Self-lubricated mantle convection: two-dimensional models. Geophys. Res. Lett. 21, 1707–1710.
Mart, Y., Aharonov, E., Mulugeta, G., Ryan, W., Tentler, T., Goren, L., 2005. Analogue modelling of the initiation of subduction. Geophys. J. Int. 160, 1081–1091.
McKenzie, D.P., 1977. The initiation of trenches. In: Talwani, M., Pitman III, W.C. (Eds.), Island Arcs, Deep Sea Trenches, and Back-Arc Basins, Maurice Ewing Ser. vol. 1. AGU, Washington, D.C., pp. 57–61.
Moresi, L., Solomatov, V., 1998. Mantle convection with a brittle lithosphere: thoughts on the global tectonic styles of the Earth and Venus. Geophys. J. Int. 133, 669–682.
Mueller, S., Phillips, R.J., 1991. On the initiation of subduction. J. Geophys. Res. 96, 651–665.
Ni, S., Gurnis, M., Helmberger, D.V., 2002. Sharp sides to the African superplume. Science 296, 1850–1852.
Ni, S., Helmberger, D.V., Tromp, J., 2005. Three-dimensional structure of the African superplume from waveform modelling. J. Geophys. Res. 161, 283–294.
Ogawa, M., 1990. Perturbation analysis of convective instability of oceanic lithosphere and initiation of subduction. J. Geophys. Res. 95, 409–420.
Peacock, S.M., Wang, K., 1999. Seismic consequences of warm versus cool subduction metamorphism: examples from Southwest and Northeast Japan. Science 286, 937–939.
Pinkerton, H., Stevenson, R.J., 1992. Methods of determining the rheological properties of magmas at subliquidus temperatures. J. Volcanol. Geotherm. Res. 53, 47–66.
Poli, S., Schmidt, M.W., 2002. Petrology of subducted slabs. Annu. Rev. Earth Planet. Sci. 30, 207–235.
Ranalli, G., 1995. Rheology of the Earth. Chapman and Hall, London, 413 pp.
Reese, C.C., Solomatov, V., Moresi, L., 1999. Non-Newtonian stagnant lid convection and magmatic resurfacing on Venus. Icarus 139, 67–80.
Regenauer Lieb, K., Yuen David, A., 2000. Fast mechanisms for the formation of new plate boundaries. Tectonophysics 322, 53.

Regenauer-Lieb, K., Yuen, D.A., Branlund, J., 2001. The initiation of subduction: criticality by addition of water? Science 294, 578–580.
Rey, P.F., Philippot, P., Thébaud, N., 2003. Contribution of mantle plumes, crustal thickening and greenstone blanketing to the 2.75–2.65 Ga global crisis. Precambrian Res. 127, 43–60.
Richard, G., Bercovici, D., Karato, S.-I., 2006. Slab dehydration in the Earth's mantle transition zone. Earth Planet. Sci. Lett. 251, 156–167.
Sandwell, D.T., Schubert, G., 1992. Evidence for retrograde lithospheric subduction of Venus. Science 257, 770–776.
Schmidt, M.W., Poli, S., 1998. Experimentally based water budgets for dehydrating slabs and consequences for arc magma generation. Earth Planet. Sci. Lett. 163, 361–379.
Smithies, R.H., Champion, D.C., Van Kranendonk, M.J., Howard, H.M., Hickman, A.H., 2005. Modern-style subduction processes in the Mesoarchean: geochemical evidence from the 3.12 Ga Whundo intra-oceanic arc. Earth Planet. Sci. Lett. 231, 221–237.
Sobolev, S.V., Babeyko, A.Y., 2005. What drives orogeny in the Andes? Geology 33, 617–620.
Sol, S., Thomson, C.J., Kendall, J.-M., White, D., Van Decar, J.C., Asudeh, I., 2002. Seismic tomographic images of the cratonic upper mantle beneath the Western Superior Province of the Canadian Shield—a remnant Archean slab? Phys. Earth Planet. Inter. 134, 53–69.
Solomatov, V.S., 2004. Initiation of subduction by small-scale convection. J. Geophys. Res. 109, B05408.
Stern, R.J., 2004. Subduction initiation: spontaneous and induced. Earth Planet. Sci. Lett. 226, 275–292.
Tackley, P.J., 2000. Self-consistent generation of tectonic plates in time-dependent, three-dimensional mantle convection simulations. 1. Pseudoplastic yielding. Geochem. Geophys. Geosyst., 1: paper-no. 2000GC000036.
Toth, J., Gurnis, M., 1998. Dynamics of subduction initiation at pre-existing fault zones. J. Geophys. Res. 103, 18053–18067.
Turcotte, D.L., Haxby, W.F., Ockendon, J.R., 1977. Lithospheric instabilities. In: Talwani, M., Pitman III, W.C. (Eds.), Island Arcs, Deep Sea Trenches, and Back-Arc Basins, Maurice Ewing Ser. vol. 1. AGU, Washington, D.C., pp. 63–69.
Turcotte, D.L., Morein, G., Roberts, D., Malamud, B.D., 1999. Catastrophic resurfacing and episodic subduction on Venus. Icarus 139, 49–54.
Turcotte, D.L., Schubert, G., 2002. Geodynamics. Cambridge University Press, Cambridge, 456 pp.
Van der Lee, S., Regenauer-Lieb, K., Yuen, D.A., 2008. The role of water in connecting past and future episodes of subduction. Earth Planet. Sci. Lett. 273, 15–27.
Zoback, M.D., et al., 1987. New evidence of the state of stress of the San Andreas fault system. Science 238, 1105–1111.